

CONF-910123--7

UCRL-JC--106272

DE91 007261

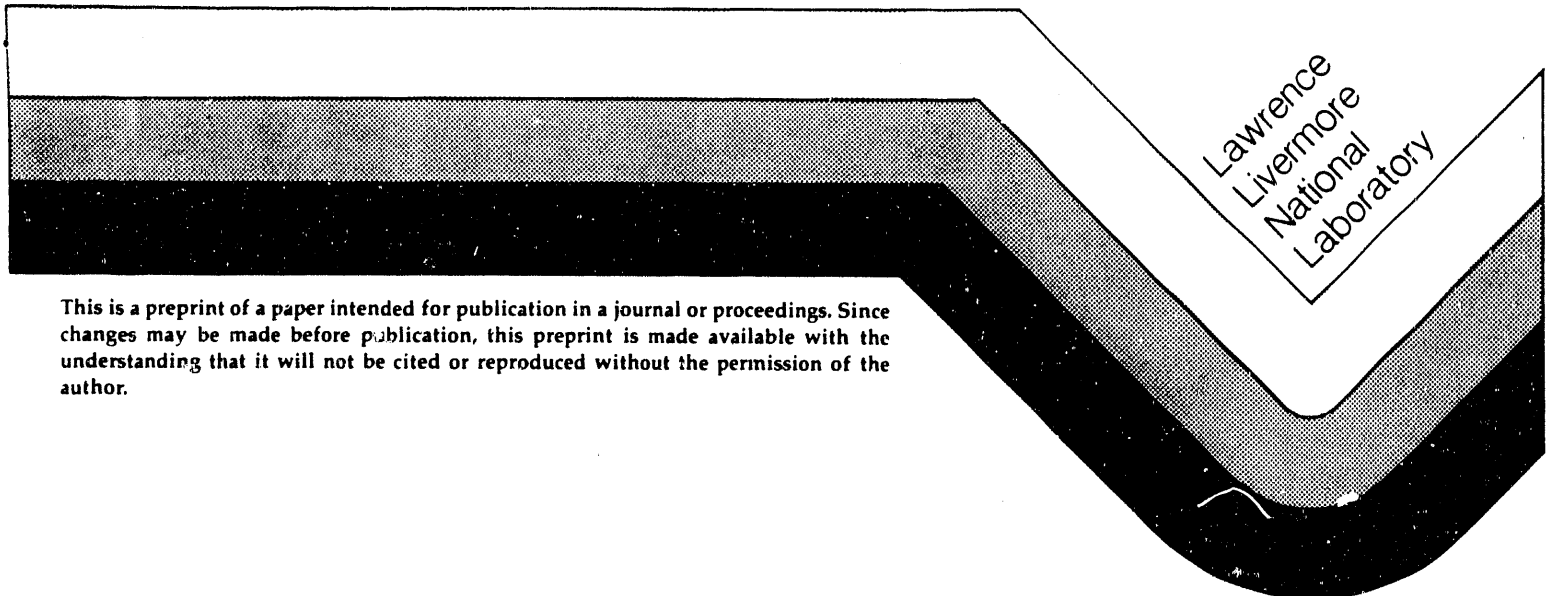
RECEIVED BY OSTI  
FEB 08 1991

Optically-Ionized Plasma Recombination  
X-Ray Lasers

P. Amendt, D.C. Eder, S. C. Wilks,  
M.J. Dunning, and C.J. Keane

This paper was prepared for publication in the proceedings of the  
SPIE's International Symposium on High Power Lasers  
Los Angeles, CA  
January 20-25, 1991

January 18, 1991



This is a preprint of a paper intended for publication in a journal or proceedings. Since changes may be made before publication, this preprint is made available with the understanding that it will not be cited or reproduced without the permission of the author.

**MASTER** *OMP*  
DISTRIBUTION OF THIS DOCUMENT IS UNLIMITED

#### DISCLAIMER

This document was prepared as an account of work sponsored by an agency of the United States Government. Neither the United States Government nor the University of California nor any of their employees, makes any warranty, express or implied, or assumes any legal liability or responsibility for the accuracy, completeness, or usefulness of any information, apparatus, product, or process disclosed, or represents that its use would not infringe privately owned rights. Reference herein to any specific commercial products, process, or service by trade name, trademark, manufacturer, or otherwise, does not necessarily constitute or imply its endorsement, recommendation, or favoring by the United States Government or the University of California. The views and opinions of authors expressed herein do not necessarily state or reflect those of the United States Government or the University of California, and shall not be used for advertising or product endorsement purposes.

## Optically ionized plasma recombination x-ray lasers

Peter Amendt, D.C. Eder, S.C. Wilks, M.J. Dunning and C.J. Keane

Lawrence Livermore National Laboratory  
University of California  
Livermore, California 94550

### ABSTRACT

Design studies for recombination x-ray lasers based on plasmas ionized by high intensity, short pulse optical lasers are presented. Transient lasing on  $n=3$  to  $n=2$  transitions in Lithium-like Neon allows for moderately short wavelengths ( $\leq 100\text{\AA}$ ) without requiring ionizing intensities associated with relativistic electron quiver energies. The electron energy distribution following the ionizing pulse affects directly the predicted gains for this resonance transition. Efficiencies of  $10^{-6}$  or greater are found for plasma temperatures in the vicinity of 40 eV. Simulation studies of parametric heating phenomena relating to stimulated Raman and Compton scattering are presented. For electron densities less than about  $2.5 \times 10^{20} \text{ cm}^{-3}$  and peak driver intensity of  $2 \times 10^{17} \text{ W/cm}^2$  at  $0.25 \mu\text{m}$  with pulse length of 100 fsec, the amount of electron heating is found to be marginally significant. For Lithium-like Aluminum, the required relativistic ionizing intensity gives excessive electron heating and reduced efficiency, thereby rendering this scheme impractical for generating shorter wavelength lasing ( $\leq 50\text{\AA}$ ) in the transient case. Following the transient lasing phase, a slow hydrodynamic expansion into the surrounding cool plasma is accompanied by quasi-static gain on the  $n = 4$  to  $n = 3$  transition in Lithium-like Neon. Parametric heating effects on gain optimization in this regime are also discussed.

### 1. INTRODUCTION

With the near-term prospect of short pulse ( $\tau \leq 100$  fsec), high intensity ( $I \geq 10^{17} \text{ W/cm}^2$ ), short wavelength ( $\lambda \sim 0.25 \mu\text{m}$ ) lasers,<sup>1</sup> a further study of their possible use in x-ray laser schemes is timely. Previously, most work has concentrated on studying the possibility of optical-field-induced ionized plasmas as recombination lasers in the quasi-static regime.<sup>2-4</sup> The quasi-static phase of x-ray lasing typically occurs over a time scale of around a hundred picoseconds or more, which is associated with a hydrodynamic time scale. By contrast, the transient phase of population inversion occurs over a much shorter radiative time scale and is characterized by a significantly smaller transition wavelength. In addition, the transient gains are ordinarily large compared to quasi-static values of gain, which generally requires that the effects of saturation be considered.

For either transient or quasi-static recombination regime, the use of optical-field-induced ionization represents a promising approach toward the development of table-top x-ray lasers. Currently, collisional ionization schemes rely on large and expensive ICF-class drivers to demonstrate x-ray lasing to ever smaller wavelengths. Despite the prodigious power requirements, lasing has recently been demonstrated in the so-called water window, which lies between the K-edges of Carbon and Oxygen ( $23.2 \text{\AA}$ - $43.7 \text{\AA}$ ).<sup>5</sup> To achieve lasing in this wavelength range is important because holographic imaging of live biological samples now becomes within technical reach.<sup>6</sup> Our purpose in this paper is to optimize the energy efficiency using optical-field-induced ionization as a basic alternative to the benchmark collisional excitation schemes. Although our study will still take us well outside of the water window, the acceptable efficiencies found will demonstrate a possibly useful and relatively compact source of short wavelength ( $\lambda_x \leq 100 \text{\AA}$ ) x-rays.

In section 2 we describe a simplified atomic kinetics model in Lithium-like ions for determining transient small-signal gains and their duration. The large values of maximum small-signal gain found necessitate a modelling of the saturation behavior; in particular we estimate the saturated intensity for a given transition and the saturation length. We then calculate the energy

efficiency as a function of electron density, temperature and beam waist size, from which an optimal set of parameters will be identified.

A large uncertainty in optical-field-induced ionization schemes for x-ray lasers is the degree to which anomalous collective heating mechanisms may undermine the entire approach. We confront this issue in section 3 by implementing an N-body simulation (ZOHAR) of laser-induced plasma behavior and searching for plasma parameters which result in minimal heating.

In section 4 we briefly discuss the quasi-static recombination phase in Lithium-like Neon within the context of parametric heating constraints. We conclude in section 5.

## 2. TRANSIENT REGIME ENERGY EFFICIENCY IN LITHIUM-LIKE NEON

A promising candidate for efficient optical-field-induced ionization x-ray lasers is Lithium-like Neon with its relatively low value of required laser intensity  $I_{\text{req}}$  ( $\sim 10^{17}$  W/cm<sup>2</sup>). The relatively low intensity required for stripping Neon to the He-like ionization state is advantageous both for its technical feasibility and because of reduced parametric heating effects. The small signal gains associated with the resonance transitions will depend strongly on the residual electron energy following passage of the driver-laser pulse, and it is important to minimize as much as possible whatever heating mechanisms there are in order to optimize the efficiency.

We begin our analysis with a simplified kinetics description of Lithium-like Neon. We identify three principal time scales in ascending order: (1) the time scale for Saha equilibration of the upper states which is assumed instantaneous, (2) the lasing or radiative time scale which defines the transient regime, and (3) the recombination time scale which is very long compared to a radiative time scale and which defines the quasi-static regime (see §4). Continuum lowering (or truncation of the higher Rydberg states) is borrowed from More:<sup>7</sup>

$$\Delta E = 2.16 \times 10^{-7} \frac{Z}{R_i} \left[ \left( 1 + \left( \frac{R_d}{R_i} \right)^3 \right)^{2/3} - \left( \frac{R_d}{R_i} \right)^2 \right], \quad (1)$$

where  $Z$  is the charge of the Lithium-like ion,  $R_d[\text{cm}] = 743.4(T_e/n_e(1+Z))^{1/2}$  is the Debye radius,  $R_i = 0.62(Z/n_e)^{1/3}$  is the ion-sphere radius,  $Z=Z+1$  is the average background plasma charge,  $T_e[\text{eV}]$  is the electron plasma temperature (which we also take as the ion temperature for simplicity),  $n_e[\text{cm}^{-3}]$  is the electron plasma density, and  $\Delta E$  is the energy shift of the continuum in eV. For the plasmas of interest here ( $T_e \sim 25$  eV,  $n_e \sim 10^{20}$ ),  $\Delta E$  is about 5 eV which corresponds to a maximum principal quantum number  $n$  of about 13 in Neon. Because the  $n=3$  to  $n=2$  resonance transition (88 Å) is our primary interest, the only practical effect on our model of the higher Rydberg states beyond about  $n=7$  is to determine the initial Helium-like Neon population given the electron density. We further assume that the  $n=2$  to  $n=4$  levels are initially empty with the top three states  $n=5,6$ , and 7 in Saha equilibrium:<sup>8</sup>

$$N_{\text{Li}}(n) = N_{\text{He}}(n=1) S(n), \quad (2a)$$

with the Saha ratio  $S_n$  given by:

$$S_n = 2.16 \times 10^{-23} n_e g(n) e^{I(n)/T_e} T_e^{3/2}, \quad (2b)$$

where  $g(n)$  is the degeneracy of level  $n$ , and  $I(n)$  is the ionization potential in eV of state  $n$ . For  $n, l \rightarrow n', l'$  electron collisional-induced transitions we use Coulomb-Born exchange collision rates when  $n, n' \leq 5$ ;<sup>9,10</sup> otherwise, the semi-empirical formulas of Sampson and Zhang are used.<sup>11</sup> The resulting detailed atomic model is then shell-averaged to obtain a hydrogenic model.

To test this simplified model we have considered the effect on the  $n=3$  and  $2$  level populations of two separate choices for the initial population of the  $n=5$  level: (a)  $N_5(0)=0$  and (b)  $N_5(t)=\text{constant}$  (or Saha). Figures (1a, b) display the statistically weighted populations for the four lowest levels along with the  $4 \rightarrow 3$  and  $3 \rightarrow 2$  gain profiles. With regard to the  $3 \rightarrow 2$  transition, we see

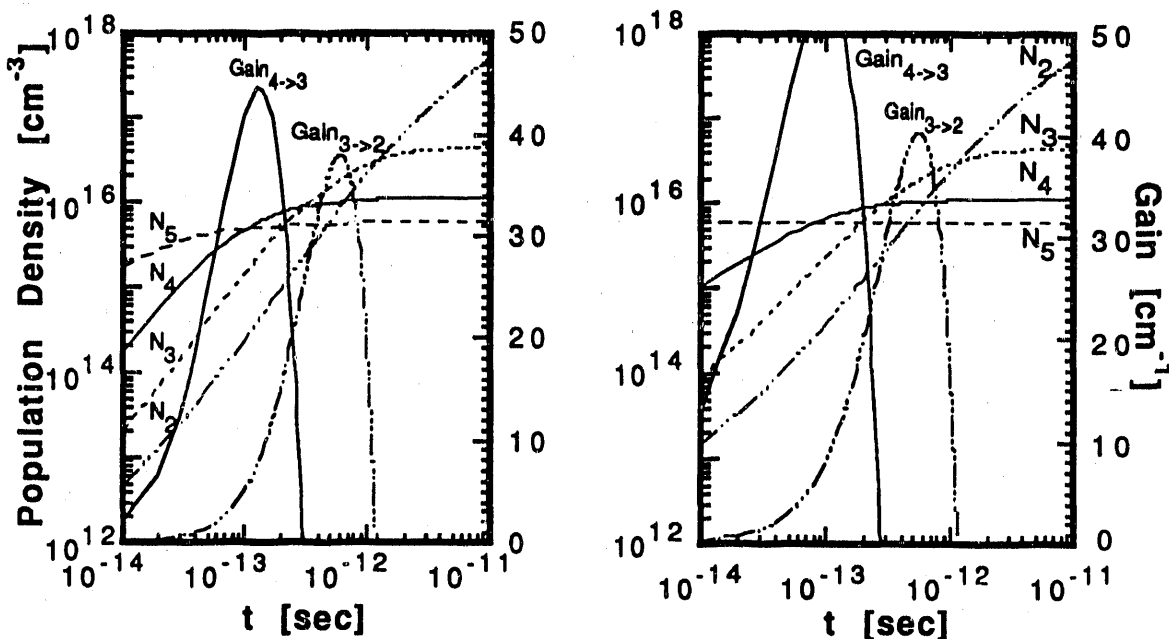


Fig. (1a,b): In the left-most figure (1a) is shown the four lowest level populations of Lithium-like Neon along with the indicated gain profiles when the  $n=5$  level is initially empty. In the right-hand figure (1b) the  $n=5$  level is assumed instead to be constant in time with population fixed at the Saha value. In both figures  $n_e = 2.5 \times 10^{20} \text{ cm}^{-3}$  and  $T_e = 25 \text{ eV}$ .

that the associated gain profile is not very sensitive to our initial choice for  $N_5(t)$ . For the  $N_5(0)=0$  case in fig. (1a), the  $n=5$  population is seen to reach the Saha value in approximately 100 fsec, which occurs well before the peak of the  $3 \rightarrow 2$  gain. We have also studied the case where  $N_5(t)$  is initially Saha populated in order to verify that  $N_5$  remains in Saha equilibrium to a high degree. In computing the gain profiles, we have considered both Doppler line broadening as well as Stark broadening as shown in fig. (2a). The Stark line width calculations are based on analytic estimates which include both ion-ion interactions and electron-ion collisions (H. Griem, private communication (1985)). We have checked these analytic line width results using a detailed Stark model of Lee,<sup>11</sup> and the agreement is satisfactorily within a factor of two for our parameters. For the densities and temperatures of interest to us the line shapes are seen to be generally dominated by Stark broadening. In fig. (2a) we have concentrated on a particular fine structure transition ( $3d_{5/2} \rightarrow 2p_{3/2}$ ; 98 Å) which has dominant gain compared to the other five transitions possible (see fig. (2b)). For the remainder of our study of transient gain in Lithium-like Neon we consider only this particular transition.

The gain associated with this resonance transition is quite large, particularly at low temperature and high density. Therefore, it is necessary that we consider the effects of saturation in this system, i.e., when the maximum small signal gain  $G$  is reduced to one-half of its value by stimulated emission. A steady-state estimate of the saturation intensity is admissible since the time scale of the processes that affect the upper laser state (primarily electron collisions with upper levels)

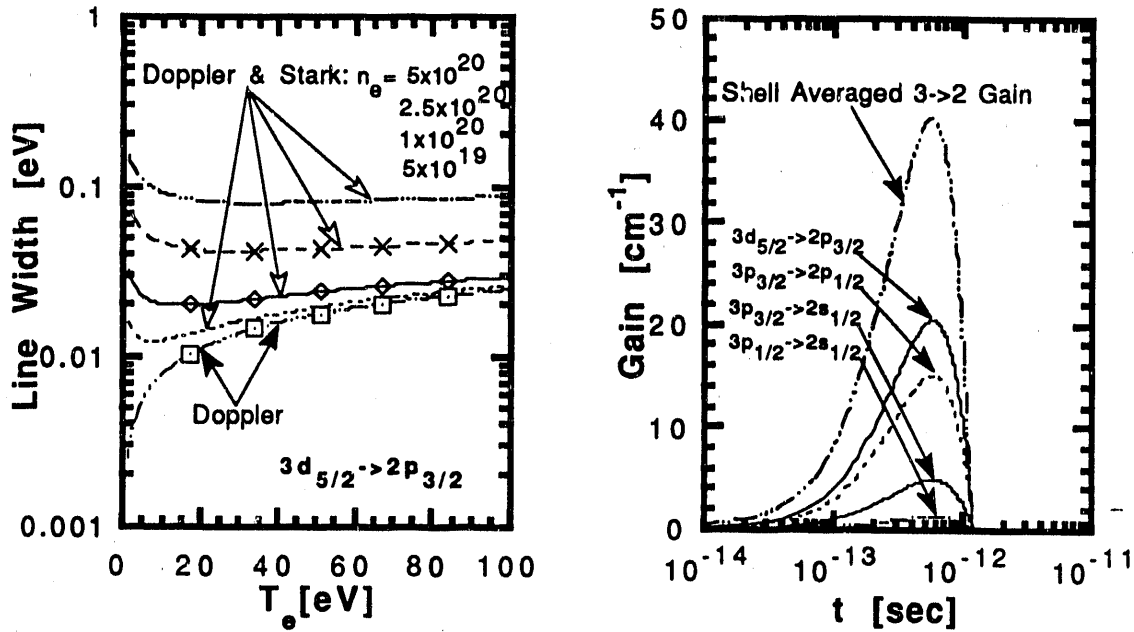


Fig. (2a,b): Shown in the left-hand figure (2a) are the Doppler and total (Doppler and Stark) line widths in Lithium-like Neon for the  $3d_{5/2} \rightarrow 2p_{3/2}$  transition. In the right-hand figure (2b) are displayed the various fine structure gain profiles for  $T_e=25$  eV and  $n_e=2.5 \times 10^{20}$  cm $^{-3}$ .

is generally short compared to the duration of the gain. A saturation mean specific (per unit frequency) intensity  $J_s$  is defined by equating the stimulated emission rate to the total exit rate from the upper state  $\gamma_{out}$ , where  $\gamma_{out}$  includes all possible non-stimulated depletion processes of the upper state, when the lower state is *empty* even in the presence of stimulated emission.<sup>13</sup> We introduce an adjustable multiplier  $\alpha \leq 1$  for the net stimulated emission rate at saturation:  $\alpha \gamma_{out}$  in order to model the stimulated emission rate with a *non-empty* lower level population. With use of the standard Einstein formula for the net emission, we obtain:

$$J_s = \left(\frac{1}{3}\right) \alpha \gamma_{out} \left[ \frac{c^2}{2h\nu^3} A_{ul} \left( 1 - \frac{N'_l g_u}{N'_u g_l} \right) \right]^{-1}, \quad (3)$$

where  $(1 - N'_l g_u / N'_u g_l)$  is the population inversion factor, the prime notation on the upper and lower fine structure populations,  $N'_u$  and  $N'_l$ , refers to their saturated values,  $g_u$  and  $g_l$  are degeneracy factors for the respective levels,  $A_{ul}$  is the spontaneous emission rate,  $\nu$  is the transition frequency,  $h$  is Planck's constant, and  $c$  is the speed of light. The factor of one-third in eq. (3) arises in order to reflect the presence of five other fine structure transitions with their respective statistical weights. Since the population flow into the upper level is the same with or without stimulated emission (stimulated absorption into the level is accounted for by using the net stimulated emission rate), the flow out must also be the same. Equating the population outward flow rates with and without stimulated emission, we have  $N_u \gamma_{tot} = N'_u \gamma_{tot} + N'_u \alpha \gamma_{out} / 3$ , where the last term is the net stimulated

emission contribution at saturation and  $N_u$  is the upper-state population at maximum small-signal gain. Defining  $\beta=1/(1+\alpha/3)$ , we find that the saturated and unsaturated upper level populations are related by  $N_u'=\beta N_u$ . Upon choosing a physically relevant relation between  $N_1'$ ,  $N_1$ ,  $N_u$ ,  $N_u'$  and  $\beta$ , we can solve for  $\beta$  such that the gain when expressed in terms of primed populations is reduced by one-half compared to its small-signal value (unprimed). For example, the choice  $N_1'=N_1+3(1-\beta)N_u/2$  assumes that all of the  $n=2$  fine structure levels are in statistical equilibrium, giving

$$\beta = \left[ \frac{1}{2} \left( 1 + \frac{N_1 g_u}{N_u g_l} \right) + \frac{3 g_u}{2 g_l} \right] / \left( 1 + \frac{3 g_u}{2 g_l} \right). \quad (4)$$

We have not considered the additional sink of upper-level population into the next lower Be-like Ne ionization state; thus, the associated gain is an underestimate since about 10% of the Li-like Ne ground state can be shown to rapidly fill the upper Rydberg states of the Be-like state by recombination.

Given a population inversion factor, we may readily find  $\beta$  from eq. (4) and thus  $\alpha$ . We generally have  $\beta$  near unity and  $\alpha$  small compared to one in strong contrast to the case of an empty lower state. Using  $\alpha$  in eq. (3) we easily obtain  $J_s$  and the saturated intensity  $I_{sat} = \Delta v J_s [2\pi^3/l n 2]^{1/2}$ , where  $\Delta v$  is the FWHM of the atomic line profile. The populations  $N_1$  and  $N_u$  are found by straightforwardly solving the system of rate equations and dividing by their respective statistical weights. In addition to the saturation intensity we need to determine the distance along the z-axis at which the amplifying intensity reaches  $I_{sat}$ ; this condition defines the saturation length  $L_{sat}$ . The saturation length is found by equating  $J_s$  with the line mean intensity  $J$ :

$$J = \left( \frac{S}{2\pi} \right) \left[ \int_0^{\tan^{-1}a/L_{sat}} \frac{(e^{GL_{sat}/\cos\theta} - 1)^{3/2}}{\left( \frac{GL_{sat}}{\cos\theta} e^{GL_{sat}/\cos\theta} \right)^{1/2}} \sin\theta d\theta + \int_{\tan^{-1}a/L_{sat}}^{\pi/2} \frac{(e^{Ga/\sin\theta} - 1)^{3/2}}{\left( \frac{Ga}{\sin\theta} e^{Ga/\sin\theta} \right)^{1/2}} \sin\theta d\theta \right], \quad (5)$$

where  $S = (2h\nu^3/c^2)/(1-g_u N_1/g_l N_u)$  is the source function,  $a$  is the lasing medium half-width, and  $\theta$  is the angle from the z axis at which the (geometric) ray propagates within the plasma. The integrands in eq.(5) represent the line integrated specific intensity which is found by first solving the transfer equation for the specific intensity  $I(\nu)$ , weighting  $I(\nu)$  by a line profile function which we take as Gaussian, and then integrating over  $\nu$ . The first integral corresponds to rays which exit the end of the lasing slab at  $z=L_{sat}$  and the second includes contributions from rays which exit from the side of the slab ( $z < L_{sat}$ ). In practice we require that the solutions for  $L_{sat}$  satisfy  $a/L_{sat} \leq 0.05$  in order to distinguish our lasing system from a high brightness noise source.

With  $I_{sat}$  and  $L_{sat}$  now known, the laser intensity  $I(z)$  is approximately given by:

$$I(z) = \left\{ \begin{array}{ll} I_{sat} \frac{z}{L_{sat}} & , z \geq L_{sat} \\ I_{sat} \frac{(e^{Gz} - 1)^{3/2} (GL_{sat} e^{GL_{sat}})^{1/2}}{[Gz e^{Gz}]^{1/2} (e^{GL_{sat}} - 1)^{3/2}} & , z \leq L_{sat} \end{array} \right\}. \quad (6)$$

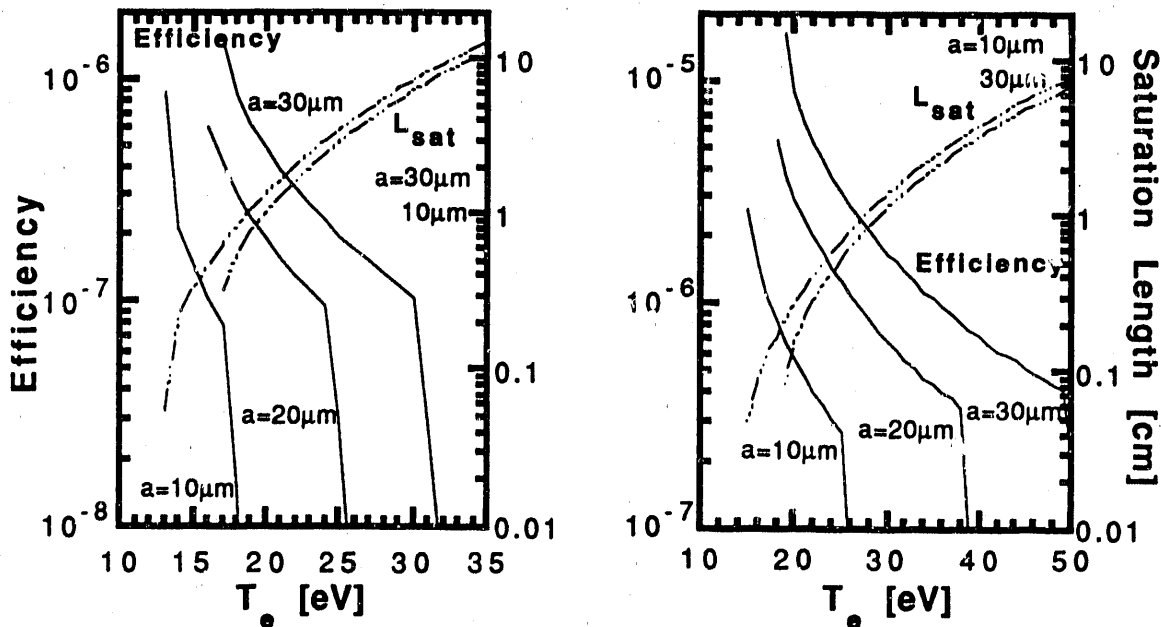
The total energy output  $E_{out}$  is obtained as follows:

$$E_{\text{out}} = I(z) \Delta\tau \pi a^2, \quad (7)$$

where  $\Delta\tau$  is the FWHM of the  $3d_{5/2} \rightarrow 2p_{3/2}$  gain profile, and  $a$  is now identified as the half-intensity radius of the ionizing laser pulse, which we assume has a Gaussian profile in the transverse direction. The effective distance of propagation of the laser pulse is limited by diffraction and is given by the confocal parameter:<sup>14</sup>

$$z = \frac{4 \pi a^2}{\lambda \ln 2}, \quad (8)$$

where  $\lambda$  is the ionizing laser wavelength. However,  $z$  cannot be so large that there is insufficient energy in the laser driver to optically ionize the plasma channel as desired. This condition sets the maximum value of  $z$  at a few centimeters (or a maximal half-intensity radius of nearly  $30 \mu\text{m}$ ) for  $\tau \sim 100$  fsec,  $I_{\text{req}} \sim 10^{17} \text{ W/cm}^2$ ,  $n_e \sim 10^{20} \text{ cm}^{-3}$  in Lithium-like Neon. The energy efficiency is defined as the ratio of output energy to input energy  $E_{\text{in}}$ , where  $E_{\text{in}} = I_{\text{req}} \tau \pi a^2$ . In figs. (3a, b) we display the energy efficiency as a function of temperature for several values of  $a$ . The left-most truncation for each



Figs. (3a,b): Energy efficiency and saturation length  $L_{\text{sat}}$  in Lithium-like Neon as a function of temperature for several values of half-intensity radius  $a$ . The electron density  $n_e$  is  $1.0 \times 10^{20} \text{ cm}^{-3}$  for the left-hand figure (3a) and  $2.5 \times 10^{20} \text{ cm}^{-3}$  for the right-hand figure (3b).

curve results from our adopted threshold saturation length  $L_{\text{sat}} > 20a$ . Also evident is a break in the slope of each curve at higher temperature indicating a threshold for intensity saturation, cf., eq. (6). The general trend of improved efficiency with increasing  $a$  is attributable to the strong scaling of the confocal parameter  $z$  with  $a$ , cf., eq. (8). The coherent energy efficiency per transverse mode is found by dividing the total energy efficiency by the number of saturated transverse modes in the system.

The number of transverse modes scales as the square of the Fresnel number  $F = 2\pi a^2/\lambda_x z$ . Therefore, the coherent energy scales as  $(\lambda/\lambda_x)^2$ , which typically corresponds to much less than one  $\mu\text{J}$  of coherent energy. Perhaps the only hope of obtaining improved coherence is to match the focussing length  $z$  with  $L_{\text{sat}}$ , thereby maximally exploiting gain discrimination effects associated with the strongest growing transverse modes. However, the corresponding efficiencies are greatly reduced as clearly shown in figs. (3a, b).

A further feature of figs. (3a, b) is the strong dependence of efficiency on temperature, particularly at low  $T_e$ , which underscores the need to minimize residual heating mechanisms. We have also plotted the efficiency as a function of electron density in fig. (4a) which indicates a very favorable trend when  $n_e$  is increased. However, this result is effectively weakened by the accompanying strong increase in parametric heating with  $n_e$  for a given pulse width which we will consider shortly. For the case of Lithium-like Aluminum ( $54 \text{ \AA}$ ) shown in fig. (4b), the required high ionizing laser intensity ( $\sim 10^{18} \text{ W/cm}^2$ ) promotes excessive parametric heating as well as low efficiency in comparison to Lithium-like Neon. In general, shorter wavelength schemes based on the transient recombination scheme require far shorter laser-driver pulse lengths ( $\tau \leq 20 \text{ fsec}$ ) than those envisioned for the near term.

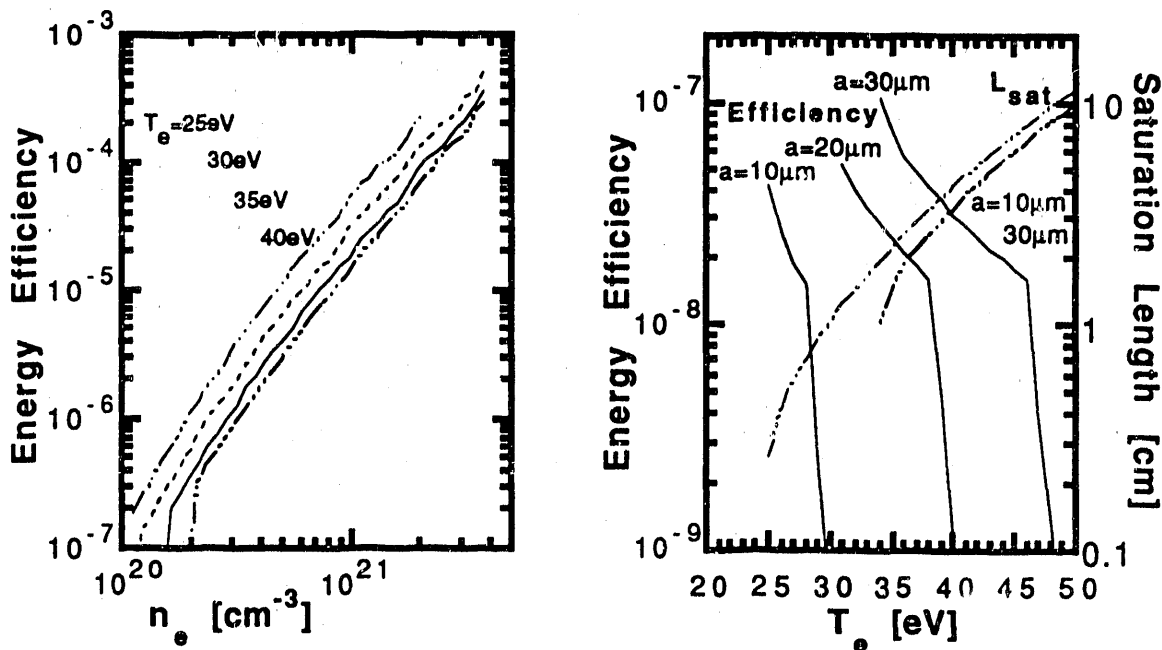


Fig. (4a,b): In the left-hand figure (4a) are shown energy efficiencies versus electron density in Lithium-like Neon for half-intensity radius  $a=25 \mu\text{m}$ . In right-hand figure (4b) are displayed energy efficiencies and saturation lengths in Lithium-like Aluminum versus electron temperature for  $n_e=2.5 \times 10^{20} \text{ cm}^{-3}$ .

### 3. PARAMETRIC HEATING EFFECTS

The recombination x-ray laser scheme requires as little residual electron heating as possible in order to generate high energy efficiencies. There are a host of heating mechanisms which can potentially plague the method:<sup>15</sup> above-threshold-ionization (ATI), strong field inverse

Bremsstrahlung, inelastic collisions, plasmon wake-field generation, and stimulated Compton or Raman scattering. Recent PIC simulations of ATI heating with space charge effects included show that this source of heating is not serious provided the plasma period is not in resonance with either the laser pulse length  $\tau$  or the laser period ( $1/\nu$ ), which we assume.<sup>16</sup> For the plasma conditions of interest to us in Helium-like Neon ( $n_e \sim 10^{20} \text{ cm}^{-3}$ ,  $\lambda \sim 0.25 \mu\text{m}$ ,  $I_{\text{req}} \sim 10^{17} \text{ W/cm}^2$ ,  $\tau \sim 100 \text{ fsec}$ ), the residual electron heating from ATI is found to be on the order of 20 eV.<sup>15</sup> For these same conditions collisional heating is evidently not an important factor in minimizing the residual energy. Inelastic collisions between electrons and Helium-like Neon ions occur too infrequently under these conditions to have a significant effect. The remaining role of parametric heating processes have long been conjectured to be potentially serious, but to our knowledge a quantitative study of their effect in optical-field-induced ionization recombination schemes has not been carried out. In this section we study the possible role of parametric heating with the aid of a 2-d PIC relativistic simulation (ZOHAR).<sup>17</sup>

Of the possible candidates for excessive parametric heating, stimulated Raman backscatter commands primary attention. The associated backscatter linear growth rate  $\gamma$  scales as:<sup>18</sup>

$$\gamma \cong \frac{1}{2} \left( \frac{v_{\text{osc}}}{c} \right) [\omega_{\text{pe}} \omega]^{1/2}, \quad (9)$$

where  $v_{\text{osc}} [\text{cm/s}] = 25.6 I_{\text{req}}^{1/2} \lambda [\mu\text{m}]$  is the electron quiver velocity,  $\omega_{\text{pe}} = 5.64 \times 10^4 n_e^{1/2}$  is the electron plasma frequency, and  $\omega = 2\pi\nu$ . For  $n_e \sim 10^{20} \text{ cm}^{-3}$ ,  $\lambda \sim 0.25 \mu\text{m}$ ,  $I \sim 10^{17} \text{ W/cm}^2$ , the growth time is on the order of 10 fsec, which is considerably less than the laser pulse lengths available. A resonantly heated electron population is subsequently formed with "temperature"  $m_e (\lambda \omega_{\text{pe}} / 4\pi)^2$  typically exceeding several keV. In figs. (5a, b) are displayed the electron distribution functions following passage of the

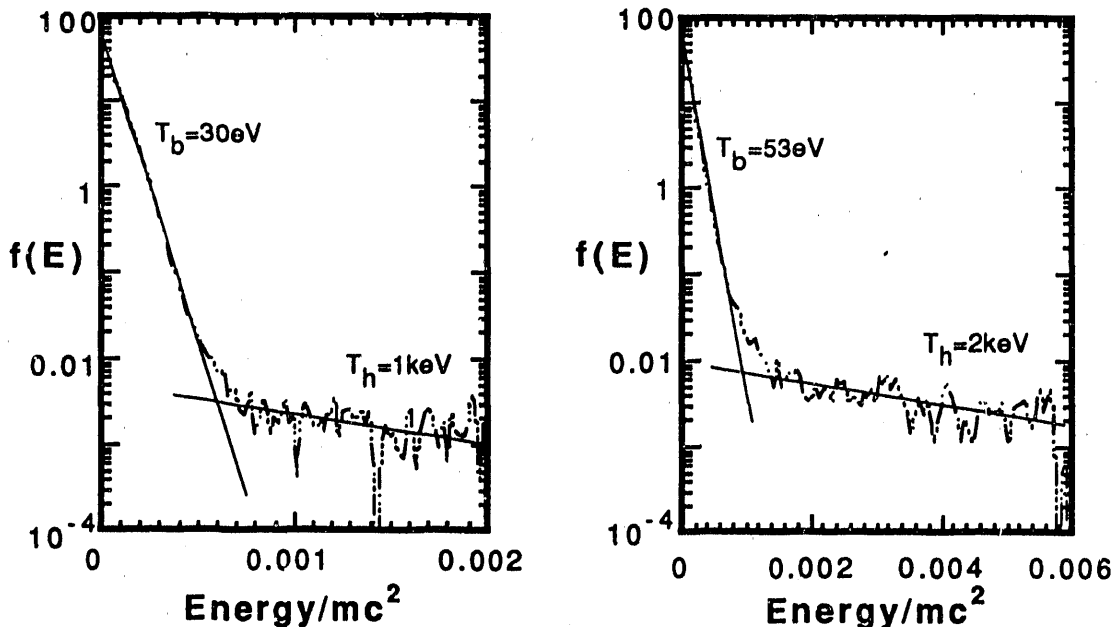


Fig. (5a,b): In the left-most figure (5a) is shown the parametrically heated electron distribution function as a function of kinetic energy normalized to the rest mass energy for an electron density  $n_e = 1.0 \times 10^{20} \text{ cm}^{-3}$ . The heated background electron temperature is denoted by  $T_b$  and the tail population temperature by  $T_h$ . In the right-hand figure (5b) the electron density is  $2.5 \times 10^{20} \text{ cm}^{-3}$ .

ionizing laser pulse for two values of electron density. We have started the simulation with an electron temperature of 25 eV to reflect supplemental heating from ATI and inverse Bremsstrahlung. In both figures the heated distribution function is seen to conveniently split into two quasi-Maxwellians each with easily identified temperature. For the higher density case of fig. (5b) a low temperature background population ( $\sim 53$  eV) is found along with a high temperature ( $\sim 2$  keV), minority population ( $\leq 0.1\%$ ). This case represents the upper limit in plasma density for which plasma heating is tolerable under the aforementioned laser conditions, cf., fig. (6a). For the lower density example in fig. (5a), parametric heating safely contributes only 5 eV in additional heating. Various signatures of the simulated parametric heating clearly indicate that Raman backscatter is principally responsible for the observed heating in the simulations. We conclude that laser pulses of around 100 fsec duration at  $0.25 \mu\text{m}$ ,  $10^{17} \text{ W/cm}^2$  require an electron density no higher than about  $2.5 \times 10^{20} \text{ cm}^{-3}$  in order for the Lithium-like Neon scheme to be practical. With these projected laser parameters shorter wavelength recombination X-ray lasers as in Lithium-like Aluminum ( $\sim 54 \text{ \AA}$ ), which require an ionizing laser of intensity  $10^{18} \text{ W/cm}^2$ , are not yet accessible as clearly demonstrated in fig. (6b) by the substantial amount of heating that occurs even for a reduced pulse length of 50 fsec.

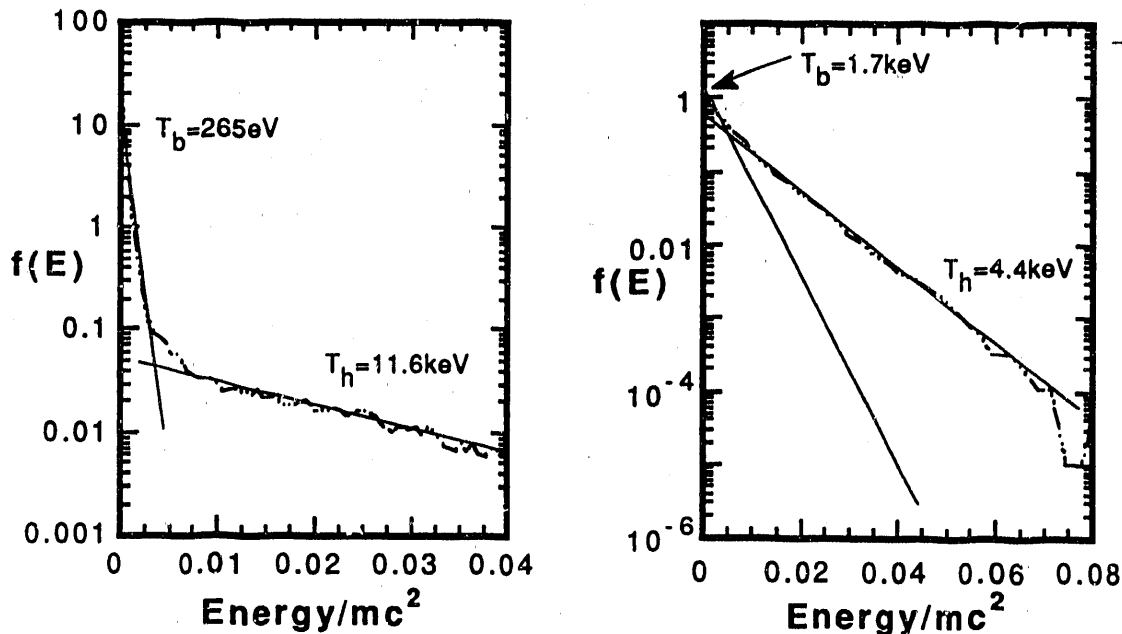


Fig. (6a,b): On the left is shown the parametrically heated electron distribution function for Lithium-like Neon with density  $n_e = 5.0 \times 10^{20} \text{ cm}^{-3}$ , intensity  $10^{17} \text{ W/cm}^2$  and pulse length 100 fsec. In the right figure (6b) the distribution function is shown for Lithium-like Aluminum for  $n_e = 2.5 \times 10^{20} \text{ cm}^{-3}$ , intensity  $10^{18} \text{ W/cm}^2$ , and pulse length of 50 fsec. In both figures  $T_b$  is the background electron temperature;  $T_h$  is the temperature of the resonantly heated electron population.

#### 4. QUASI-STATIC GAIN IN RECOMBINATION X-RAY LASERS

Following the brief transient phase of population inversion, the plasma enters a slow expansion and cooling phase which defines the quasi-static regime of recombination lasing. Under

suitable plasma conditions, population inversion may arise and persist for hundreds of picoseconds. For Lithium-like Neon the principal candidate transition is  $4 \rightarrow 3$  with a wavelength of 262 Å.

One advantage of quasi-static recombination lasing is the long duration of the population inversion compared to the transient episode, thereby giving potentially larger energy efficiencies. However, the corresponding wavelengths are comparatively large and require the use of higher Z ions in order to compete with wavelengths characteristic of the transient scheme. Unfortunately, the associated intensities required for optical-field-induced ionization are prohibitively high from the point of view of parametric heating. For example, in fig. (6b) an excessive amount of heating is seen to occur in Lithium-like Aluminum ( $4 \rightarrow 3$ ;  $\lambda_x = 154 \text{ Å}$ ) for only a 50 fsec pulse length. Generally, the onset of gain in the quasi-static phase of recombination requires somewhat less initial density than in the transient case which is beneficial from the standpoint of parametric heating. However, the stronger scaling of Raman backscatter growth rates with driving-laser intensity, cf. eq. (9), means that accessing shorter wavelengths with optical-field-induced ionization is more easily accomplished in the transient regime with use of lower Z materials. Although quasi-static recombination lasing can tolerate higher temperatures for population inversion onset, the constraints imposed by minimal parametric heating ( $T_e < 200 \text{ eV}$ ) still favor transient recombination lasing as the preferred use of optical-field-induced ionization.

## 5. CONCLUSION

In this paper we have studied the possible energy efficiency of a 98 Å recombination x-ray laser based on Lithium-like Neon operating in the transient regime. With the near-term prospect of 100 fsec, 0.25  $\mu\text{m}$ ,  $10^{17} \text{ W/cm}^2$  driving lasers we have shown that efficiencies of up to  $10^{-6}$  are possible after allowing for parametric heating effects. The extension of the method to shorter wavelengths as in Lithium-like Aluminum ( $\lambda_x = 54 \text{ Å}$ ) requires significantly higher ionizing intensities which are characterized by excessive parametric heating. Improved efficiencies are possible for the Lithium-like Neon scheme by both decreasing the laser pulse length to reduce parametric heating and increasing the electron density.

## 6. ACKNOWLEDGMENTS

We are grateful to A.B. Langdon for use of his ZOHAR code and to N. Bardsley, W. Kruer, R. Lee, J. Lindl, R. London, S. Maxon, J. Nash, and M. Rosen for useful discussions. This work was performed under the auspices of the U.S. Department of Energy by Lawrence Livermore National Laboratory under contract No. W-7405-ENG-48

## 6. REFERENCES

1. M. Pessot, J. Squier, G. Mourou, D.J. Harter, *Opt. Lett.* **14**, 797 (1989); P. Georges, F. Salin, F. Estable, G. Roger, A. Brun, *Ultrafast Phenomena VII*, C.B. Harris, E.P. Ippen, G.A. Mourou, A.H. Zewail, Eds. (Springer-Verlag, Berlin, 1990), pp. 48-50; F.G. Patterson, M.D. Perry, R. Gonzales, and E.M. Campbell, In *Femtosecond to Nanosecond High-Intensity Lasers and Applications*, E. M. Campbell, Ed. (SPIE, Bellingham, 1990), pp. 2-18; D.J. Harter, M. Pessot, J.A. Squier, J. Nees, P. Bado, G.A. Mourou, *ibid*, pp. 19-28; W. Tighe, C.H. Nam, J. Goldhar, L. Meixler, J. Robinson, E. Valeo, and S. Suckewer, *ibid*, pp. 29-39; H.C. Kapteyn, A. Sullivan, H. Hamster, R.W. Falcone, *ibid*, pp. 75-81.
2. J. Peyraud and N. Peyraud, *J. Appl. Phys.* **43**, 2993 (1972).
3. N.H. Burnett and P.B. Corkum, *J. Opt. Soc. Am.* **6B**, 1195 (1989).
4. C.J. Keane, J.N. Bardsley, L. daSilva, N. Landen, and D. Matthews, In *Femtosecond to Nanosecond High-Intensity Lasers and Applications*, E. M. Campbell, Ed. (SPIE, Bellingham, 1990), pp.190-195.
5. B.J. MacGowan, S. Maxon, L.B. Da Silva, D.J. Fields, C.J. Keane, D. L. Matthews, A.L. Osterheld, J.H. Scofield, G. Shimkaveg, and G.F. Stone, *Phys. Rev. Lett.* **65**, 420 (1990).
6. R.A. London, M.C. Rosen, and J.E. Trebes, *Appl. Opt.* **28**, 3397 (1989).
7. R.M. More, *J. Quant. Spec. Rad. Trans.* **27**, 345 (1982).

8. A. Klisnick, A. Sureau, H. Guennou, C. Möller, and J. Virmont, *Appl. Phys.* 50B, 153 (1990).
9. L.B. Golden, R.E.H. Clark, S.J. Goett, and D.H. Sampson, *Ap. J. Suppl.* 45, 603 (1981).
10. R.E.H. Clark, D.H. Sampson, and S.J. Goett, *Ap. J. Suppl.* 49, 545 (1982).
11. D.H. Sampson and H. Zhang, *Ap. J.* 335, 516 (1988).
12. R.W. Lee, *J. Quant. Spec. Rad. Trans.* 40, 561 (1988).
13. R.A. London, *Phys. Fluids* 31, 184 (1987).
14. A.F. Siegman, *Lasers* (Mill Valley, CA, University Science Books, 1986).
15. N.H. Burnett and G.D. Enright, *IEEE J. Quant. Electron.* QE-26, 1797 (1990).
16. B.M. Penetrant and J.N. Bardsley, *Phys. Rev. A*, in press (1991).
17. A.B. Langdon and B.F. Lasinski, *Methods in Computational Physics*, J. Killeen et al., Eds. (New York, N.Y., Academic Press, Vol. 16, 1976).
18. W.B. Kruer, *The Physics of Laser Plasma Interactions* (Addison-Wesley, New York, 1988).

**END**

**DATE FILMED**

03 / 05 / 91

